

Echo-Planar Imaging of Intravoxel Incoherent Motion¹

The recently established single-shot technique of echo-planar imaging of intravoxel incoherent motion (IVIM) for determining and imaging the variations of microscopic motions of water has been applied to studies of water perfusion in phantoms and to *in vivo* studies of diffusion and perfusion in cat and human brains. The phantom results demonstrate that perfusion levels comparable with those found *in vivo* have easily observable and reproducible effects on signal amplitude that are consistent with previous IVIM theory. Reliable measurements of the diffusion coefficient in various types of brain tissue have been obtained. The results for white matter are consistent with the existence of anisotropic diffusion in oriented bundles of myelinated nerve fibers. The results for gray matter can be fitted to the IVIM theory and suggest a value of up to 14% for the fraction of the signal contributed by randomly perfusing fluid in normal cerebral cortex.

Index terms: Blood, flow dynamics • Blood vessels, MR studies, 17.1214 • Brain, MR studies, 10.1214 • Brain, perfusion • Cerebral blood vessels, flow dynamics • Cerebral blood vessels, MR studies, 17.1214 • Cerebrospinal fluid, flow dynamics • Cerebrospinal fluid, MR studies • Magnetic resonance (MR), echo planar

Radiology 1990; 177:407-414

¹ From the Biomedical Engineering and Instrumental Program, National Center for Research Resources (R.T., L.K.H., J.P.), and the Department of Diagnostic Radiology, Warren G. Magnuson Clinical Center (D.L.B.), National Institutes of Health, Bethesda, Md, and from General Electric Medical Systems, Waukesha, Wis (J.M., R.V.). From the 1989 RSNA scientific assembly. Received March 29, 1990; revision requested May 25; revision received July 18; accepted July 20. Address reprint requests to R.T., Bldg 10, Rm B1D125, National Institutes of Health, Bethesda, MD 20892.

© RSNA, 1990

See also the editorial by Le Bihan (pp 328-329) and the article by Chenevert et al (pp 401-405) in this issue.

SINCE the pioneering work of Le Bihan et al (1-3) interest in the physiologic and pathologic information based on knowledge of the motion of body fluids at the cellular level has grown rapidly. Such motions have been classified as intravoxel incoherent motion (IVIM) (2) and intravoxel coherent motion (IVCM) (4). IVIM can be further analyzed as diffusion, which arises from the brownian motion of individual molecules moving with large random thermal velocities, and perfusion, which describes the pseudorandom flow at low velocities of blood moving along the finely divided structures of the capillaries. To the extent that perfusive flow is anisotropic, as in the highly oriented capillary beds characteristic of skeletal muscle, it is categorized as IVCM.

Diffusion and perfusion variations both represent bulk manifestations of histologic and physiologic differences in tissue at a microscopic level. If the size of a cell, for instance, is smaller than the distance that a water molecule travels by diffusion during the time of observation in bulk water, the diffusion coefficient may be found to be reduced; we speak of "restricted diffusion." Variations in the transverse relaxation time T2 in vegetable tissue, where the cell wall is almost impermeable to water transport, have been successfully associated with restricted diffusion in differing cell sizes (5,6), and there are some reports of similar effects in animal tissue, although such cell membranes are quite permeable to water (7). The relative viscosity and proportions of intra- and extracellular water can also cause variations in the diffusion coefficient. Thus, it is likely that

studies of diffusion alone, if it can be accurately measured, could play a major role in diagnosis of tissue abnormalities such as those associated with stroke and cancer.

The clinical and research possibilities offered by a study of perfusion are even wider. Since regional cerebral blood flow is closely correlated with brain functional activity (8), truly noninvasive dynamic studies of brain neural organization may be possible, and the origins of functional deficit in trauma or cerebral infarction might be rapidly assessed.

Despite these significant opportunities, progress in the imaging of IVIM has not been entirely satisfactory. The most serious problem has been that the technique for sensitizing a multipulse magnetic resonance (MR) imaging sequence to microscopic flows also gives it great sensitivity to bulk motions, such as cardiac-cycle-related pulsations, involuntary movements, and flow of cerebrospinal fluid. The method also makes extreme demands on imaging hardware stability, and the large magnetic field gradients that it is advisable to use can cause eddy currents in surrounding conducting structures (9), with severe consequences for image interpretability. Of course, large eddy currents with a short time constant rule out any kind of rapid imaging technique.

Presented here is an attempt to avoid this problem in the study of the diffusion of water and perfusion in the human brain. This is achieved by using a low-eddy-current gradient configuration to acquire single-shot images via echo-planar imaging (EPI) (10), which, because the entire image dataset is captured in less than 0.1

Abbreviations: CSI = chemical-shift imaging, EPI = echo-planar imaging, IVCM = intravoxel coherent motion, IVIM = intravoxel incoherent motion, MBEST = modulus blipped echo-planar single-pulse technique, RF = radio frequency, ROI = region of interest, S/N = signal-to-noise ratio, 2DFT = two-dimensional Fourier transform.

second, show no visible trace of motion artifact.

IMAGING THEORY

Diffusion Imaging

The effects of molecular diffusion on spin echoes have been studied since the early days of MR (11–13). In the presence of a magnetic field gradient, random spin displacements produce random dephasings that destructively interfere with each other, resulting in an attenuation of the spin-echo amplitude. Due to the gaussian profile of brownian motion, this attenuation S/S_0 has an exponential dependence, such that

$$S/S_0 = \exp(-bD), \quad (1)$$

where D is the diffusion coefficient (considered here as isotropic) and b is a factor that depends only on the magnetic field gradients applied before data acquisition.

The concept of "diffusion imaging" is much more recent (1,2,14). Due to the multiple gradient pulses used in an imaging sequence, the expression for b must be generalized and now takes the form

$$b = \int_0^{TE} |\mathbf{k}(t)|^2 dt \quad (2)$$

with

$$\mathbf{k}(t) = \gamma \int_0^t \mathbf{G}(t') dt', \quad (3)$$

where in a spin-echo sequence the sign of $\mathbf{G}(t')$ is reversed for $t' > TE/2$ (TE = echo time). Due to the vector nature of this relation, the contributions b_x , b_y , and b_z for each coordinate axis can be considered separately. If diffusion is anisotropic, the different components of the diffusion tensor must be taken into account:

$$S/S_0 = \exp\left(-\sum_{(i=x,y,z)} b_i D_i\right). \quad (4)$$

For a typical two-dimensional Fourier transform (2DFT) imaging sequence, the b factor remains low, typically less than $1 \text{ sec} \cdot \text{mm}^{-2}$, so the diffusion effect is negligible (for $D = 2.10^{-3} \text{ mm}^2 \text{ sec}^{-1}$, the diffusion coefficient of water at room temperature, $S/S_0 = 0.998$). To increase the sensitivity of an imaging sequence to diffusion, it is necessary to incorporate additional gradient pulses into the sequence (1,2,14). It then becomes possible to compute diffusion

images (ie, maps where the diffusion coefficient is displayed in each pixel) by using two or more of such sequences differently sensitized to diffusion (1,2).

Different variants of diffusion imaging have been proposed. With the spin-echo scheme, it is possible to vary the strength or the duration of the diffusion-sensitizing gradients (15,16), or their direction, to enhance anisotropic diffusion effects (17). Other schemes have been used, such as the stimulated-echo sequence (18) or the steady-state free-precession technique (19–21).

IVIM Imaging

The concept of diffusion imaging can be extended to encompass IVIM imaging if we consider the signal attenuation produced by any additional incoherent motion of spins inside each voxel. The attenuation is increased, compared with that caused by diffusion alone, and the dependence on diffusion gradient may be different. However, anatomic data suggest that the microcirculation of blood in capillaries can be seen as a pseudodiffusion process, at least in such tissues as the brain (3). We then have to combine the effects of diffusion and microcirculation, which occur simultaneously in each voxel. Using a simple approach, one obtains for the signal attenuation (3)

$$S/S_0 = (1-f) \exp(-bD) + f \exp(-bD^*), \quad (5)$$

where D and D^* are, respectively, the true diffusion coefficient and the pseudo-diffusion coefficient and f is the fractional volume occupied in the voxel by flowing spins, or perfusion factor. This simple two-compartment model neglects exchanges between the capillaries and the tissue and differences in relaxation between these two compartments. Nevertheless, a biexponential variation of the signal attenuation versus the b factor manifests the presence of incoherent motion other than diffusion. Furthermore, estimates of D , D^* , and f may be made by fitting the signal intensities obtained in images acquired with different b factors to the above equation.

Signal-to-noise ratio (S/N) considerations require the use of many data points in order to estimate these parameters with reasonable accuracy. It is likely that only single-shot techniques, such as EPI, will allow the acquisition of enough data within the

short time compatible with clinical use.

Motion Artifact

In conventional multipulse imaging, even without diffusion gradients, motion artifact can arise when the object, or part of the object, is displaced by a distance Δx , say, between successive acquisition cycles. The subsequent echo is phase modulated by the function $\exp(i k \Delta x)$, where k is the phase-space coordinate, so there is a discontinuity between this and the previous echo. Once the complete dataset has been collected, and the 2DFT performed to produce an image, such a discontinuity manifests itself as the familiar ghost artifact distributed in the phase-encode direction seen in many images. Since the magnitude of the discontinuity depends on k (a first-order effect), the power in the ghost images is not usually large.

However, the situation is much worse when the large gradients used in diffusion imaging are applied, or when the object to be imaged is moving rapidly, as in conventional abdominal imaging. The signal now depends on the velocity of coherent and incoherent flows within the object, as well as its displacement. For no artifact to appear, all of these variables must be the same at each echo acquisition. Cardiac gating is of some benefit, especially in brain imaging, but noncyclic changes in blood flow and perfusion, cerebrospinal fluid flow, and involuntary patient motion have often caused unreliable results (21,22). The phase factor introduced by a variation of velocity of Δv between successive echoes is now of the form $\exp(i \gamma G \Delta v t^2)$, where t is the time during which the gradients are applied. There is a discontinuity at all values of k (a zeroth-order effect), and the ghost images may have a large enough amplitude to make calculation of the diffusion image meaningless.

With EPI, on the other hand, the entire set of echoes that is Fourier-transformed to form an image is collected in a single acquisition period of 25–100 msec. No discontinuity can possibly arise between successive data points, and hence there can be no motion-derived ghosting. Even if there were bulk motion as large as several voxel widths during this short acquisition, only blurring and banding of the image would be likely to result. Such velocities are not normally encountered in the brain. Rap-

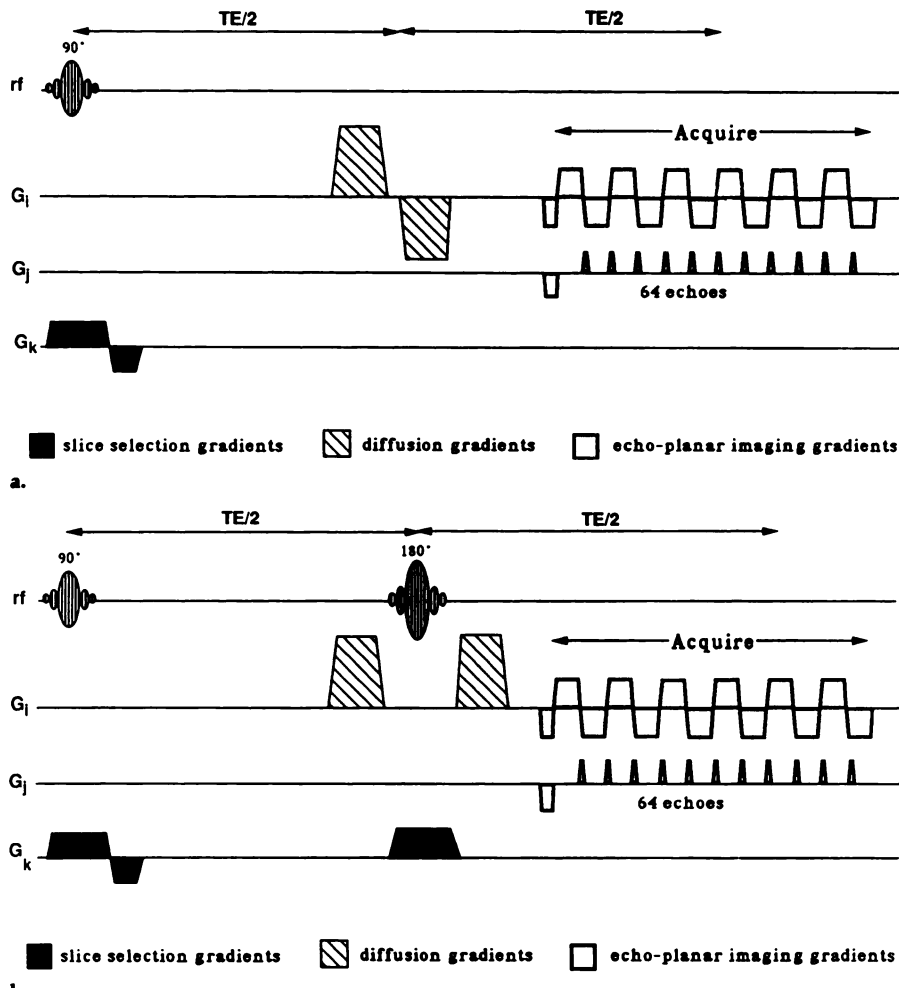


Figure 1. (a) Gradient-echo diffusion-weighted EPI sequence. (b) Spin-echo diffusion-weighted EPI sequence. Typical duration of diffusion gradients was 20 msec per lobe.

idly flowing blood in larger vessels and cerebrospinal fluid in the third ventricle and the aqueducts have a characteristic variation in appearance over the cardiac cycle during EPI, but no distributed motion artifact is ever observed, as has been repeatedly demonstrated in cardiac EPI (23). The pulsatile component of capillary flow in the brain is, of course, negligible (24).

The IVIM-EPI Sequence and Its Gradient-Echo Counterpart

It is quite straightforward to sensitize EPI (10) to diffusion and perfusion. The simplest EPI technique to implement on commercial MR equipment is the MBEST (modulus blipped echo-planar single-pulse technique) sequence (25,26), either in its spin-echo (27) or gradient-echo (28) form. The arrangement of the diffusion gradient pulses is slightly different in each case, as shown in Figure 1. Since EPI describes only a method for acquiring image data, it is com-

patible with any technique for preparing the spin magnetization that creates diffusion contrast (29).

Special Hardware Requirements for IVIM-EPI

For EPI capability, an MR imager must have certain unusual features. The most stringent of these are concerned with maximum gradient strength and gradient switching speed. It is also necessary to use radio-frequency (RF) transmitter and receiver coils that cannot support eddy currents induced by the rapidly switched gradients. In practice this means that RF coils with extensive areas of copper, such as the Alderman-Grant design (30), are unsuitable, and designs such as the birdcage or saddle-coil type are favored.

To obtain echo-planar images, either actively shielded, low-inductance gradient coils (10,31,32) or a gradient-coil insert that is very much smaller than the magnet bore of an imaging system (33) must be used. A

rise time of less than 200 μ sec is desirable; the rise time of 1 msec or more typically found with commercial unshielded gradient coils makes EPI impossible.

MATERIALS AND METHODS

Sequence Implementation

Both of the IVIM-EPI sequences described above have been successfully implemented on a 1.5-T whole-body imager (Signa; GE Medical Systems, Milwaukee) and on 2-T and 4.7-T medium-bore chemical-shift imaging (CSI) systems (GE Medical Systems). On all of these imaging machines, 128×128 images of phantoms with long T_2 s have been obtained, but the data acquisition rate currently available makes the acquisition window too long for *in vivo* work at this resolution, giving rise to unacceptable image distortion. The studies reported here were performed at 64×64 resolution.

In the course of image reconstruction, special care must be taken to ensure that the data are correctly aligned in k -space after alternate echoes are time reversed. If this is not done properly, an aliasing ghost appears halfway across the field of view from the desired image. For the CSI systems the onset of sampling was carefully adjusted, and the dataset was shifted left until the ghost disappeared (29). For the Signa system a different strategy was adopted. A reference image, with phase-encode gradients switched off, was obtained at the start of each set of image acquisitions. Suitably transformed data from the reference image were used to perform a phase correction on the subsequent image data. This has the same effect as properly aligning the echoes for Fourier transformation and also corrects to some extent the effects of field inhomogeneity.

The CSI results shown in this article were obtained by means of a set of shielded gradients (Acustar 260; GE Medical Systems) that gave a maximum gradient of 40 mT m^{-1} , with a rise time of 170 μ sec. A 64×64 resolution enabled a minimum field of view of 40 mm to be achieved, giving a pixel size of $0.625 \times 0.625 \times 2.0$ mm.

The standard Signa gradient coils have a good ratio of current efficiency to inductance. However, the current amplifiers that drive them cannot deliver sufficient current to allow EPI of a reasonably sized field of view. For this reason, novel local gradient coils, which give a much larger z gradient, were designed and built, initially as inserts for the standard quadrature head RF coil. Having a diameter of only 27 cm, such coils are much more efficient than the whole-body gradient set and have a much lower inductance of only about $100 \mu\text{H}$. Their only important limitation is that transaxial EPIs cannot be obtained.

The first such coil had the standard Maxwell configuration, resulting in a us-

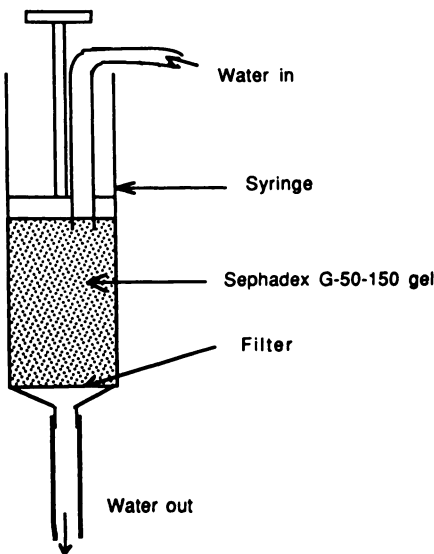


Figure 2. Perfusion phantom used for test of IVIM theory. Typical perfusion rate was 60 mL/100 g per minute.

able volume only 14 cm across. Since it interacted little with the RF coil, however, it could be used as planned for imaging of the brain, and initial testing of the EPI sequences were successfully performed with its aid.

To enlarge the usable volume, however, a second distributed-arc gradient coil was built from a target field design (34), with an efficiency of 42.9 mT/m per 100 A. This gave a usable volume of 20-cm diameter, with an inductance similar to the first coil, but it interacted severely with the standard RF coil. It was necessary, therefore, to construct and use a new RF coil (a simple saddle coil) mounted on the interior wall of this gradient coil.

Diffusion and Perfusion Experiments in Phantoms

To confirm that IVIM-EPI is capable of determining diffusion and perfusion characteristics accurately and reliably, a series of experiments was performed on water-containing phantoms, with use of the 2-T CSI imaging system for convenience. Results from a simple bottle of undoped water (29) compared well with results from the spin-echo IVIM spin-echo sequence previously validated (2,3).

A series of experiments was then conducted with use of the gradient-echo version of the echo-planar sequence and a perfusion phantom. This consisted of a syringe (Fig 2) filled with a chromatography gel (Sephadex G-50-150, Sigma Chemical, St Louis), a polyacrylamide gel with excellent MR characteristics (3). Perfusion water flow rates of 10–100 mL/100 g per minute can easily be established in this medium. The individual beads, which contain many reentrance cavities with dimensions similar to those of human brain cells, are 50–150 μm in diameter, a distance comparable with inter-

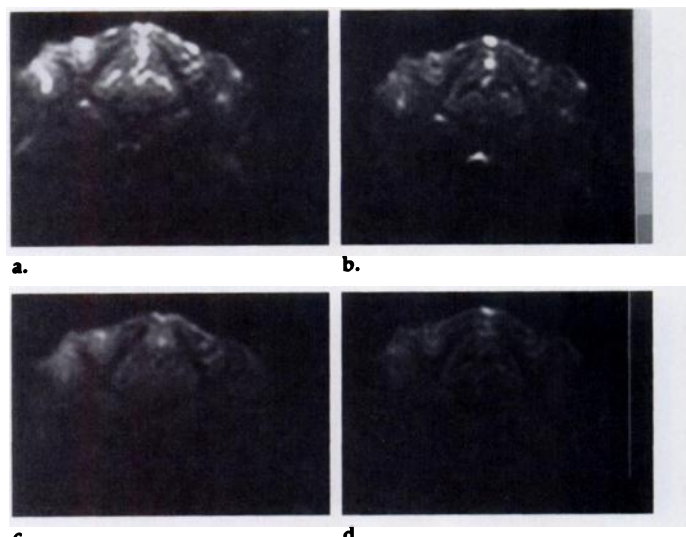


Figure 4. Cat brain coronal images acquired with the gradient-echo EPI sequence on the CSI system. (a) Five minutes before death, the diffusion gradient is 0.0 $\text{mT} \cdot \text{m}^{-1}$. (b) Ten seconds after cessation of heartbeat, the diffusion gradient is 0.0 $\text{mT} \cdot \text{m}^{-1}$. (c) Four minutes before death, the diffusion gradient is 30 $\text{mT} \cdot \text{m}^{-1}$. (d) Three minutes after death, the diffusion gradient is 30 $\text{mT} \cdot \text{m}^{-1}$.

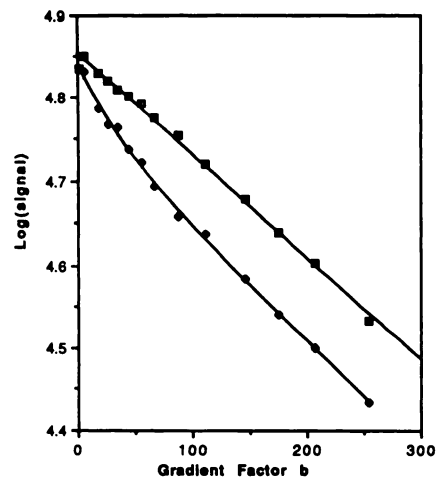


Figure 3. Typical results from a perfusion phantom experiment. □ = perfusion off, ♦ = perfusion on (with biexponential fit). Data were taken from a region of interest (ROI) in center of phantom. Section thickness was 2 mm, and acquisition time was 94 msec. The horizontal axis is shown in units of $\text{sec} \cdot \text{mm}^{-2}$.

pillary spacing in brain tissue. When wet, the gel is quite compressible and must be handled with care to avoid clogging.

Cat Brain Studies

Using the same 2-T CSI system, we obtained IVIM-EPI images of the brains of three cats. A 15-cm-diameter saddle coil was used as a transmitter, and the MR signal was observed by means of a 5-cm-diameter surface coil, positioned between the ears to obtain the maximum possible S/N. The coils were decoupled by means

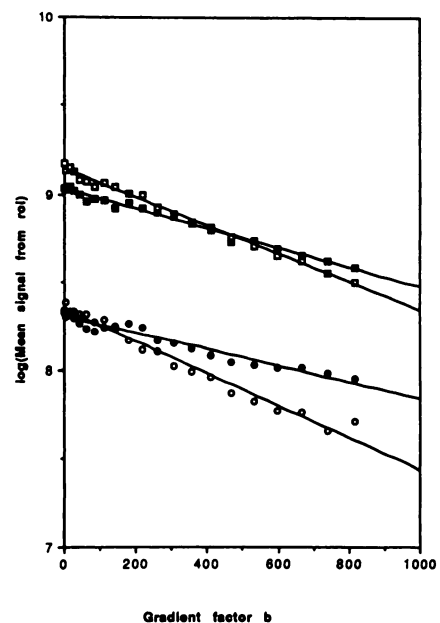


Figure 5. Results from cat brain experiment. Note dramatic change of slope for both gray and white matter within 5 minutes of death. □ = gray matter (live), ○ = white matter (live), ■ = gray matter (dead), ● = white matter (dead).

of diodes. The cats were anesthetized with isoflurane, paralyzed with succinylcholine, kept warm by means of a heating jacket, and maintained on a respirator until the conclusion of the experiment. Hourly checks of blood gas levels were performed; these were found to be stable and normal. The rectal temperature of the second cat was continuously monitored and found to remain constant within 0.4°C, even up to 0.5 hour after death. Be-

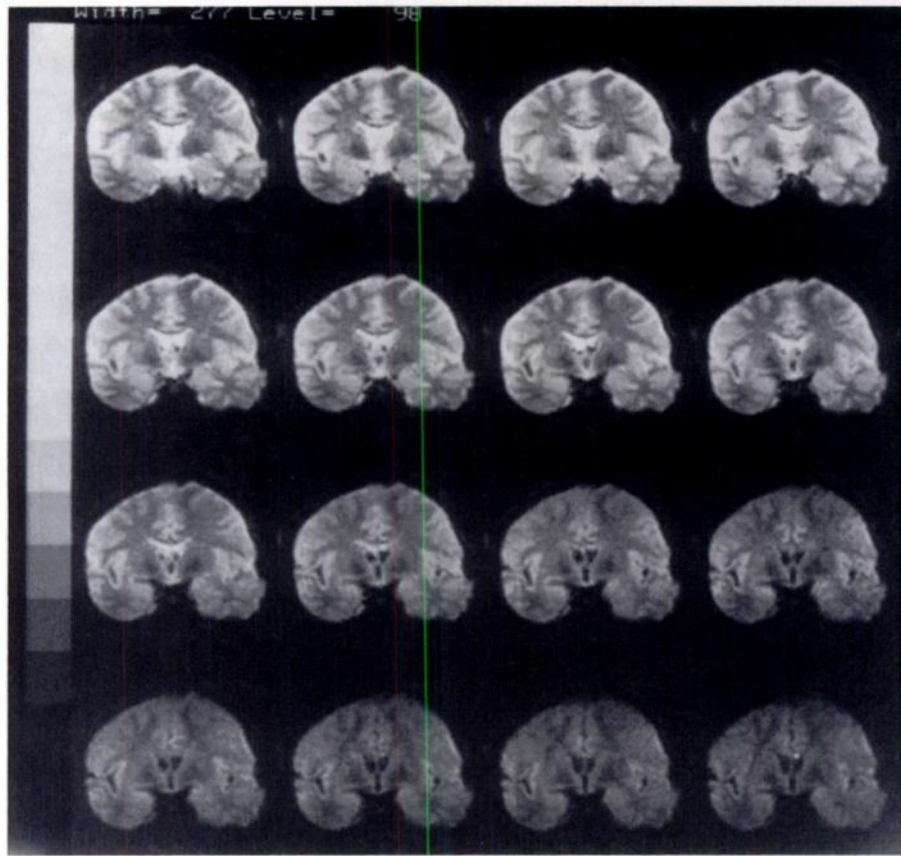


Figure 6. Sixteen diffusion-weighted coronal echo-planar images of the brain of a volunteer. These are 64×64 -pixel images with a field of view of 16 cm and thus an in-plane resolution of 2.5×2.5 mm. The section thickness was 10 mm. The diffusion gradients varied from 0 to $38 \text{ mT} \cdot \text{m}^{-1}$, and the duration of each lobe was 20 msec.

fore the experiment was concluded, each cat was killed with 3 mL of T-61 euthanasia solution (Hoechst-Roussel [Agrivet], Somerville, NJ) administered into the femoral vein, in accordance with National Institutes of Health animal care guidelines. The uniquely high speed of EPI made it possible to obtain brain images within seconds of death, which was indicated by the cessation of heartbeat and loss of blood pressure.

Studies in Human Brain

By use of the small head gradient coil described earlier, coronal diffusion-weighted echo-planar images were obtained of the heads of volunteers and patients. Results from patients are not shown here. To obtain good-quality images, it was necessary to use the spin-echo version of the MBEST sequence. The S/N for a 64×64 image with a 16-cm field of view and 10-mm section thickness was measured to be about 50:1, allowing quantitative measurements to be made of the effects of diffusion on the MR signal. The spatial resolution in plane is 2.5 mm. Cardiac gating was sometimes used to avoid possible effects due to changes in the contrast of moving blood.

RESULTS

Phantoms

Typical results are shown in Figure 3. The effect on the MR signal of a flow rate of as little as $60 \text{ mL}/100 \text{ g}$

per minute is quite dramatic. Use of the Marquardt nonlinear least-squares fit algorithm shows that the points are well fitted by a biexponential variation with b , and the resultant perfusion parameters are entirely reasonable, confirming previously published results obtained with a 2DFT spin-echo sequence (3).

Cat Brain

Typical EPI images, again acquired by means of the gradient-echo EPI sequence, are shown in Figure 4. These show 64×64 -pixel coronal sections of 3-mm section thickness and 40-mm field of view, interpolated by zero filling to 128×128 pixels. The decrease in signal from top to bottom arises from the nonuniform sensitivity of the surface coil. The total acquisition time for each image was 140 msec, the largest echo of the train of 64 echoes occurring at about 100 msec after the initial RF pulse. This gives considerable T2 weighting to the images, and some distortion owing to imperfect shimming is also evident.

Figure 4a was acquired when the cat was alive, and Figure 4b was acquired 40 seconds after injection of T-61 euthanasia solution, that is, 10 seconds after cessation of heartbeat. All imaging parameters were kept identical, and the cat head was firmly clamped by the surface coil mounting. There is an evident loss of signal intensity upon death, most clearly visible in regions of gray matter. This rapid change of intensity was observed in each of the three cats studied. No convincing explanation exists at this time, but it may be noted that after brain ischemia, intracellular cerebral sodium increases on a similar time scale (Eleff S, unpublished data, 1990), more quickly than the changes in cell metabolites commonly observed by means of MR spectroscopy. Figure 4c and 4d, for which diffusion gradients of $30 \text{ mT} \cdot \text{m}^{-1}$ were applied, were acquired before and after death, respectively. A complete set of diffusion-weighted images was obtained within 5 minutes of death, and typical results from specific regions of interest are shown in Figure 5. The drop in gray matter signal is seen to be accompanied by a change of slope of the attenuation curve, that is, a decrease in the diffusion coefficient. This decrease of slope was consistently observed in both gray and white matter.

Calculated values of the diffusion coefficient ($\times 10^{-3} \text{ mm}^2 \text{ sec}^{-1}$) in different regions of feline brain tissue are as follows: gray matter (live), 0.82 ± 0.05 ; gray matter (dead), 0.55 ± 0.02 ; white matter (live), 0.94 ± 0.04 ; and white matter (dead), 0.47 ± 0.03 . Only one orientation of diffusion gradient (y) was used in this study. Within the field of view of the surface coil used, most of the nerve fibers constituting the white matter ran roughly parallel to the diffusion gradient, and hence the range of relative orientations of the diffusion gradient and these fibers was too small for the anisotropy previously reported (17) to be observable. Furthermore, the data for the gray matter show too much scatter for the curvature related to perfusion (which should appear at relatively low values of b) (35) to be measurable.

Human Brain

A sequence of 16 images of the brain of a volunteer is shown in Fig-

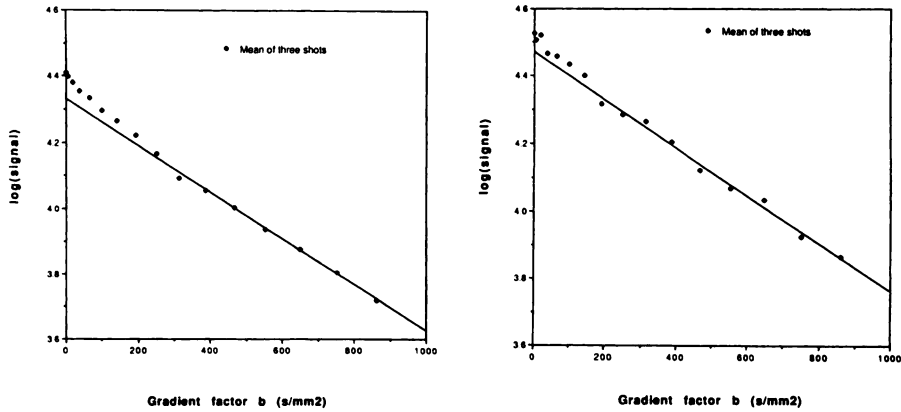
ure 6, for values of G_d from 0 to 38 mT m^{-1} . Since the echo time was 100 msec, the image contrast is dominated by T2 effects, as with the cat brain images. These 64×64 images, with a field of view of 16 cm, have an in-plane resolution of 2.5 mm. The section thickness was 10 mm.

Gray and white matter can be clearly distinguished. The attenuation with increasing diffusion gradient for white matter can be seen to vary spatially, being most rapid when the nerve fibers run parallel to the diffusion gradient (here applied in the z direction, ie, parallel to the brain stem), and least when the fibers are perpendicular to this direction. There is no visible motion artifact on any of these images, even for the highest values of diffusion gradient, and thus reliable estimates can be made of the diffusion coefficients of various types of human brain tissue.

Quantitative measurements of various ROIs were performed, and the results are shown graphically in Figures 7-9. Each data point represents the mean of the ROI pixel intensity from three successive imaging shots, with a repetition time of 3 seconds. Each ROI included at least four pixels. Since the single-shot pixel S/N was approximately 50, the expected S/N in the averaged ROI data was about 170. On each plot the straight line represents a least-squares fit to the last eight data points, where the effect of diffusion predominates. In further analysis, the entire set of points was fitted to a biexponential variation (Eq [5]) by means of a nonlinear least-squares fit to evaluate the possible contribution of perfusion in the curvature of the initial part of the plot. The results are shown in the Table.

Figures 7 and 8 show data from two gray matter ROIs, one in the region of the amygdala and the other in the insula. Figure 9 shows, correspondingly, the data from two white matter ROIs, with contrasting fiber orientation. The difference in diffusion coefficient is clearly observable. In the plots for three of these regions, a curvature is clearly seen.

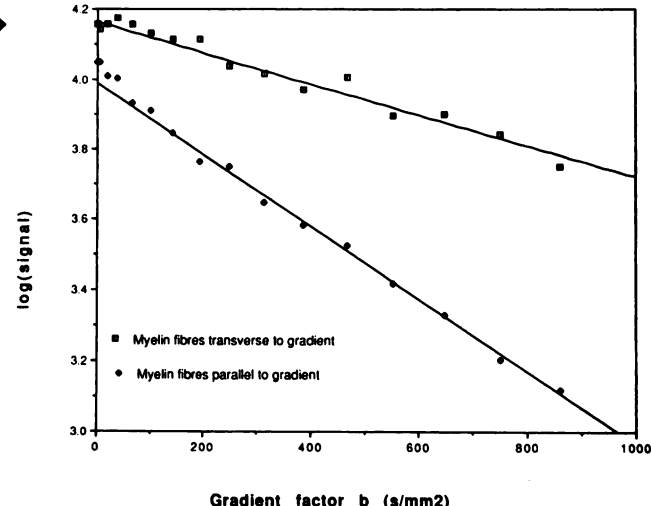
Figure 10a shows the diffusion map of a coronal section of the brain of a different volunteer; image brightness is directly proportional to the diffusion coefficient. This image was derived by performing a pixel-by-pixel iterative nonlinear least-squares fit of eight echo-planar images with different b factors, all greater than $300 \text{ sec} \cdot \text{mm}^{-2}$, to Equation (1). Areas of the white matter



7.

Figures 7, 8. (7) Graph of signal attenuation plotted against b factor, from a region of gray matter in the amygdala of the human brain. (8) Graph of signal attenuation plotted against b factor, from a region of gray matter within the insula.

Figure 9. Graph of signal attenuation plotted against b factor, from two different regions of white matter in frontal lobe, with main fiber direction parallel (\diamond) to the diffusion-gradient direction (superior frontal gyrus) and perpendicular (\square) to the gradient direction (superior temporal gyrus).



corresponding to fiber orientations parallel to and perpendicular to the diffusion gradient are indicated by arrows. The differences in diffusion coefficient are easily visible and correlate well with anatomy. Figure 10b shows the amplitude image derived from the same set of raw images and displays gray-white contrast normal for such a long echo time.

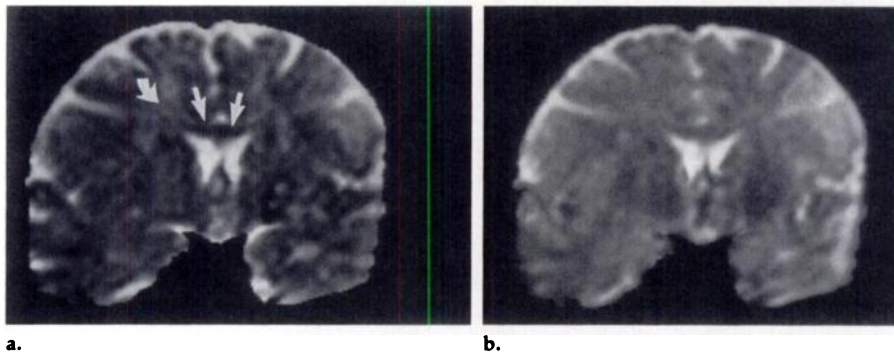
DISCUSSION

The results from the experimental work described here show that single-shot diffusion imaging is feasible. Data were reproducible from run to run, typically with a pixel variation of less than 2%, and the variation in diffusion coefficient calculated from corresponding ROIs in the volunteers studied was less than 20%. The cat data showed similar consistency. Certain technical points deserve discussion.

The most noticeable limitation of

EPI in the implementation described here is the low image resolution. This comes about, given the efficient gradient coils now available, from the relatively low data-acquisition rate available on the commercial MR equipment used. Analog-to-digital converters are currently available that are considerably faster than those installed in most systems, and we anticipate that an EPI resolution of 128×128 , or even 128×256 , with the same total acquisition time and field of view, will soon be feasible by upgrading our whole-body MR system.

An extremely well-shimmed magnet is necessary if good quality images are to be obtained by means of EPI, especially with the gradient-echo sequence. When an additional delay of 40 msec was introduced into the spin-echo EPI sequence after the 90° pulse to allow time for the diffusion gradients to be applied, the normal shim quality of our magnet (15-18 Hz across a head-sized phantom)



a. b.

Figure 10. (a) Diffusion image of a coronal section of the brain of a volunteer. Section thickness, 10 mm; field of view, 16 cm; resolution, 64×64 . This image was obtained by performing a nonlinear least-squares fit of Equation (1) to the last eight images of a 16-image echo-planar dataset obtained with increasing b factor. The spatial variation of the parameter D is displayed as a gray scale. Curved arrow indicates a region of white matter where the fibers are parallel to the diffusion gradient and thus shows a relatively high diffusion coefficient. The straight arrows indicate an area (corpus callosum) where the fibers are perpendicular to the diffusion gradient and shows a low diffusion coefficient. The image background has been set to zero to improve clarity. (b) Amplitude image corresponding to (a) showing the spatial variation of the amplitude factor S_0 . Contrast is clearly different from that seen on diffusion image and corresponds precisely to the contrast normally found in a spin-echo brain image with an echo time of 130 msec and a repetition time of 4 seconds.

Results from Human Brain Study

Tissue	Diffusion Coefficient ($\times 10^{-3} \text{ mm}^2 \text{ sec}^{-1}$)	Perfusion Fraction (%)
Gray matter		
Amygdala	0.66 ± 0.06	10.9 ± 4.0
Insula	0.68 ± 0.08	6.9 ± 5.3
White matter		
Temporal lobe, fibers perpendicular to diffusion gradient	0.43 ± 0.03	0.0006 ± 0.002
Frontal lobe, fibers parallel to diffusion gradient	1.00 ± 0.05	7.9 ± 2.3

was still found to be adequate to produce artifact-free images. Some residual geometrical distortion could be seen (Fig 6), especially in the vicinity of the paranasal sinuses. However, when the gradient-echo sequence was used, the unrefocussed effects of field inhomogeneity resulted in images of unacceptably poor quality.

To obtain reliable measurements of the diffusion coefficients of tissue *in vivo*, it is useful to obtain each image of a set of diffusion-weighted images at the same phase of the cardiac cycle by cardiac gating. The reason for this is that the EPI contrast of blood undergoing rapid, pulsatile flow in the larger vessels changes with blood velocity (24). Thus, in the absence of cardiac gating, when such a vessel is included in the ROI within which the diffusion coefficient is calculated, the experimental points on the attenuation curve can show considerable scatter. With cardiac gating, the scatter should be reduced, as observed in some of the studies made.

We now discuss the significance of the diffusion results reported. The

diffusion coefficient directly reflects the local environment of the water molecules responsible for the MR image. A lower diffusion coefficient implies either a higher local viscosity, which can arise from a decrease in temperature (36), a different balance between intra- and extracellular water, or the presence of barriers restricting molecular motion. There is little doubt that the cause of the variations we have observed within human brain white matter is the extreme anisotropy of the water environment in this tissue (17).

According to a simple model of white matter, water molecules may move unhindered long distances along the nerve-fiber direction but only a few microns perpendicular to this direction. If this medium had the viscosity of pure water at body temperature, the root mean square displacement during the time that the diffusion gradients were applied would be about $16 \mu\text{m}$. It is easy to see how the factor as large as two observed in the variation of diffusion coefficient in white matter could

have come about.

By contrast, the diffusion coefficient in gray matter shows little spatial variation in cat or human brain. Thus it would appear that the water environment in gray matter is considerably more isotropic. This is consistent with histologic evidence, showing a wider range of orientations of cell structures within the size of a voxel.

We now consider the more contentious and subtle question of perfusive blood flow along the capillary network. The most accurate and complete data for human brain so far obtained come from this study. In white matter, the signal intensity is low because of the heavy T2 weighting in the images obtained, and thus there is considerable scatter in the ROI data. For the region where the fibers lie parallel to the diffusion gradient, some curvature is visible on the attenuation plot. Curvature can also be seen in the results for gray matter, from which a perfusion factor of 6%–12% may be deduced. This effect is real and statistically significant, but the experimental scatter in the data points makes it difficult to quantitate accurately. Whether it varies with hypercarbia or brain functional activity awaits further investigation. This would clarify the link between the measured perfusion factor and actual microcirculatory flow. To reduce the scatter in the data it will be necessary to use larger ROIs or to average results from a larger number of images, which must be done after the image modulus is taken, to avoid possible phase interference effects arising from system instability.

Comparing the results for human and cat brain, we find reasonable consistency. The ranges of values of the diffusion coefficients for gray and for white matter overlap, if the cat postmortem data are excluded. These latter data are strikingly different and will not be discussed here. It should be noted that, because death causes many simultaneous changes in tissue properties that do not appear to be well understood, the experiment of killing the animal is not a suitable method of testing the IVIM theory of perfusion imaging (3).

CONCLUSION

Single-shot EPI enables precise, reproducible measurement of diffusion coefficients of human brain tissue *in vivo* without confusing motion artifacts. Furthermore, the rapidity and ease of acquiring images of adequate

quality facilitate far more detailed analyses of the attenuation curve than possible previously. Effects have been observed on the MR signal that are consistent with those predicted to be caused, according to the Le Bihan theory, by the superimposed perfusive motion of blood in capillaries. Further improvements in data analysis should lead to observations of changes in the IVIM parameters associated with brain function.

The excellent time resolution of EPI has enabled the observation of rapid changes in diffusion characteristics, which have been noted after death in the brain of a cat. If these changes are associated primarily with ischemia, it is likely that IVIM-EPI will be of great clinical benefit in diagnosis and treatment of cerebrovascular disease and other abnormalities involving the microcirculation. ■

Acknowledgments: We acknowledge use of the facilities of the NIH In Vivo NMR Center and thank Chrit Moonen, PhD, for helpful advice and Daryl Despres, Steve Merritt, and A. Scott Chesnick for technical assistance. We also thank Scott Eleff, PhD, for useful discussions and for making available unpublished observations regarding sodium MR during ischemia in a dog model.

References

- Le Bihan D, Breton E. Imagerie de diffusion in-vivo par resonance magnetique. *C R Acad Sci [II]* 1985; 15:1109-1112.
- Le Bihan D, Breton E, Lallemand D, Grenier P, Cabanis E, Laval-Jeantet M. MR imaging of intravoxel incoherent motions: application to diffusion and perfusion in neurologic disorders. *Radiology* 1986; 161:401-407.
- Le Bihan D, Breton E, Lallemand D, Aubin M-L, Vignaud J, Laval-Jeantet M. Separation of diffusion and perfusion in intravoxel incoherent motion imaging. *Radiology* 1988; 168:497-505.
- Young IR, Hall AS, Bryant DJ, et al. Assessment of brain perfusion with MR imaging. *J Comput Assist Tomogr* 1988; 12:721-727.
- Brownstein KR, Tarr CE. Importance of classical diffusion in NMR studies in biological cells. *Phys Rev A* 1979; 19:2446-2453.
- Whittall KP, MacKay AL. Quantitative interpretation of NMR relaxation data. *J Magn Reson* 1989; 84:134-152.
- Hansen JR. Pulsed NMR study of water mobility in muscle and brain tissues. *Biochem Biophys Acta* 1971; 230:482-486.
- Roy CS, Sherrington CS. On the regulation of the blood supply of the brain. *J Physiol* 1890; 11:85-108.
- Turner R, Bowley RM. Passive screening of switched magnetic field gradients. *J Phys E: Sci Instrum* 1986; 19:876-879.
- Mansfield P. Multi-planar image formation using NMR spin echoes. *J Phys C: Sol State Phys* 1977; 10:L55-L58.
- Hahn EL. Spin echoes. *Phys Rev* 1950; 80:580-594.
- Carr HY, Purcell EM. Effects of diffusion on free precession in nuclear magnetic resonance experiments. *Phys Rev* 1954; 94:630-635.
- Stejskal EO, Tanner JE. Spin diffusion measurements: spin echoes in the presence of a time-dependent field gradient. *J Chem Phys* 1964; 42:288-292.
- Taylor DG, Bushell MC. The spatial mapping of translational diffusion coefficients by the magnetic resonance imaging technique (abstr). In: Book of abstracts: Society of Magnetic Resonance in Medicine 1988; Vol 1. Berkeley, Calif: Society of Magnetic Resonance in Medicine, 1988; 612-613.
- Ahn CB, Lee SY, Nalcioglu O, Cho ZH. An improved nuclear magnetic resonance diffusion imaging method using an optimised pulse sequence. *Med Phys* 1986; 13:789-793.
- Thomsen C, Ring P, Henrikson O. In vivo measurement of water self-diffusion by magnetic resonance imaging (abstr). In: Book of abstracts: Society of Magnetic Resonance in Medicine 1988. Vol 2. Berkeley, Calif: Society of Magnetic Resonance in Medicine, 1988; 890.
- Moseley ME, Cohen Y, Mintorovitch J, et al. Early detection of regional cerebral ischemia in cats: comparison of diffusion- and T2-weighted MRI and spectroscopy. *Magn Reson Med* 1990; 14:330-346.
- Merboldt KD, Haenick W, Frahm J. Self-diffusion NMR imaging using simulated echoes. *J Magn Reson* 1985; 64:479-486.
- Le Bihan D. Intravoxel incoherent motion imaging using steady-state free precession. *Magn Reson Med* 1988; 7:346-351.
- Le Bihan D, Turner R, McFall JR. Effects of intra-voxel incoherent motions (IVIM) in steady state free precession (SSFP) imaging: application to molecular diffusion imaging. *Magn Reson Med* 1989; 10:324-337.
- Merboldt KD, Bruhn H, Frahm J, Gyngell ML, Hänicke W, Diemling M. MRI of 'diffusion' in the human brain: new results using a modified CE-FAST sequence. *Magn Reson Med* 1989; 9:423-429.
- Chenevert TL, Brunberg JA, Schielke GP. Quantitative improvement of in vivo tissue perfusion and diffusion imaging (abstr). In: Book of abstracts: Society of Magnetic Resonance in Medicine 1989. Vol 1. Berkeley, Calif: Society of Magnetic Resonance in Medicine, 1989; 62.
- Doyle M, Turner R, Cawley M, et al. Real-time cardiac imaging of adults at video frame rates by magnetic resonance imaging. *Lancet* 1986; 2:682.
- Pawlak G, Rackl A, Bing RJ. Quantitative capillary topography and blood flow in the cerebral cortex of cats: an in vivo microscopic study. *Brain Res* 1981; 208:35-58.
- Johnson G, Hutchinson JMS. The limitations of NMR recalled-echo imaging techniques. *J Magn Reson* 1985; 63:14-30.
- Howseman AM, Stehling MK, Chapman B, et al. Improvements in snapshot nuclear magnetic resonance imaging. *Br J Radiol* 1988; 61:822-828.
- Avram HE, Crooks LE. Effect of self-diffusion on echo-planar imaging (abstr). In: Book of abstracts: Society of Magnetic Resonance in Medicine 1988; Vol 2. Berkeley, Calif: Society of Magnetic Resonance in Medicine, 1988; 980.
- Turner R. Perfusion studies and fast imaging. In: Rescigno A, Boicelli A, eds. *Cerebral blood flow*. New York: Plenum, 1988; 245-258.
- Turner R, Le Bihan D. Single-shot diffusion imaging at 2.0 Tesla. *J Magn Reson* 1990; 86:445-452.
- Alderman DW, Grant DM. An efficient decoupler coil design which reduces heating in conductive samples in superconducting spectrometers. *J Magn Reson* 1979; 36:447-451.
- Mansfield P, Chapman B. Active magnetic screening of gradient coils in NMR imaging. *J Magn Reson* 1986; 66:573-576.
- Roemer PB, Edelstein WA, Hickey JS. Self-shielded gradient coils. In: Book of abstracts: Society of Magnetic Resonance in Medicine 1986. Vol 3. Berkeley, Calif: Society of Magnetic Resonance in Medicine, 1986; 1067.
- Blackband S, Chatham JC, O'Dell W, Day S. Echo-planar imaging of isolated perfused rat hearts at 4.7 T: a comparison of Langendorff and working heart preparations. *Magn Reson Med* 1990; 15:240-245.
- Turner R. A target field approach for optimal coil design. *J Phys D: Appl Phys* 1986; 19:L147-L151.
- Le Bihan D, Moonen CTW, Van Zijl PCM, Pekar J, DesPres D. Evaluation of water molecular diffusion and blood microcirculation in the cat brain at 4.7 tesla (abstr). In: Book of abstracts: Society of Magnetic Resonance in Medicine 1989. Vol 2. Berkeley, Calif: Society of Magnetic Resonance in Medicine, 1989; 1051.
- Le Bihan D, Delannoy J, Levin RL. Temperature mapping with MR imaging of molecular diffusion: application to hyperthermia. *Radiology* 1989; 171:853-857.